INFLUENCE OF CYLINDRICAL ANISOTROPY OF WOOD AND LOADING CONDITIONS ON OFF-AXIS STIFFNESS AND STRESSES OF A BOARD IN TENSION PERPENDICULAR TO GRAIN

EINFLUSS DER ZYLINDRISCHEN ANISOTROPIE DES HOLZES UND DER BELASTUNGSBEDINGUNGEN AUF DIE OFF-AXIS STEIFIGKEIT UND DIE SPANNUNGEN EINES BRETTQUERSCHNITTS BEI QUERZUGBEANSPRUCHUNG

INFLUENCE DE L'ANISOTROPIE CYLINDRIQUE DU BOIS ET DES CONDITIONS DE CHARGEMENT SUR LA RIGIDITE "OFF-AXIS" ET LES CONTRAINTES D'UNE SECTION DE PLANCHE CHARGEE EN TENSION PERPENDICULAIRE A LA FIBRE

Simon Aicher Gerhard Dill-Langer

SUMMARY

In general, the anisotropic continuum modelling of solid wood and especially of glulam is performed on the basis of quasi isotropic material behaviour within the cross-section of a beam. The neglect of the actual conical or approximately cylindrical anisotropy of wood has only minor impact on computed stresses parallel to grain. However, substantial differences are obtained for stresses perpendicular to the grain, as revealed only recently. Deviating from solutions based on isotropic or orthotropic constitutive laws within the cross-section, the actual cylindrical resp. polar orthotropic behaviour results in pronounced stress gradients along cross-sectional width.

In this paper the mechanical behaviour of a board cross-section subjected to tension perpendicular to the grain acting at the wide faces is investigated. As material law, cylindrical resp. polar orthotropic behaviour according to a realistic sawing pattern of the board is assumed. Emphasis is laid on the effect of different loading conditions.

It is demonstrated that the mechanical behaviour of a board in transverse loading is strongly dependant on the boundary conditions, which in dif-

ferent ways restrict resp. enable the coupling of normal and shear stress in the imposed off-axis loading mode. A simple analytic model for the determination of apparent MOE perpendicular to grain perceives the board cross-section as composed of springs arranged in parallel. The analytic result corresponds perfectly with FEM results for boundary conditions present at mid-height of a glulam cross-section.

ZUSAMMENFASSUNG

Im allgemeinen erfolgt die anisotrope Kontinuums-Berechnung von Vollholz und speziell von Brettschichtholz unter Zugrundelegung quasi isotropen Materialverhaltens innerhalb der Querschnittsebene des Trägers. Die Vernachlässigung der tatsächlichen konischen bzw. angenähert zylindrischen Anisotropie des Holzes hat lediglich geringen Einfluß auf die rechnerischen Spannungen parallel zur Faserrichtung. Ausgeprägte Unterschiede ergeben sich jedoch zufolge neuerer Untersuchungen für die Spannungen senkrecht zur Faserrichtung. Abweichend von Ergebnissen, die auf isotropen oder orthotropen konstitutiven Beziehungen innerhalb der Querschnittsebene beruhen, ergeben sich bei Berücksichtigung des tatsächlichen zylindrisch bzw. polar orthotropen Materialgesetzes ausgeprägte Spannungsgradienten über die Querschnittsbreite.

Im vorliegenden Aufsatz wird über das mechanische Verhalten eines Brettquerschnitts, der normal zu den Breitseiten durch Zug senkrecht zur Faserrichtung beansprucht wird, berichtet. Das Materialgesetz wird als zylindrisch bzw. polar orthotrop, basierend auf einem realistischen Jahrringverlauf innerhalb eines Brettquerschnitts angenommen. Ein Schwerpunkt der Untersuchungen liegt auf der Bestimmung des Einflusses unterschiedlicher Belastungsrandbedingungen.

Es läßt sich zeigen, daß das mechanische Verhalten des Brettes bei transversaler Beanspruchung ausgeprägt von den Randbedingungen abhängt, die in unterschiedlicher Weise die Normal-Schubspannungskopplung im aufgeprägten „off-axis" Belastungsfall behindern bzw. ermöglichen. Ein einfaches analytisches Modell zur Bestimmung des scheinbaren Elastizitätsmoduls senkrecht zur Faserrichtung beruht auf der Idealisierung des Querschnitts durch parallel- geschaltete Federn. Das analytische Ergebnis stimmt ausgezeichnet mit Finite Element Resultaten für Randbedingungen, die im mittleren Bereich der Querschnittshöhe eines Brettschichtholzquerschnitts vorliegen, überein.

RESUME

En général, le calcul du continuum anisotrope du bois resp. du bois lamellé est réalisé sur la base du comportement de matériau quasi isotrope dans la coupe transversale d'une poutre. La négligence de l'anisotropie conique ou cylindrique du bois n'a qu'une faible une influence sur les contraintes parallèles à la fibre. Par contre, comme il a été constaté récemment, des différences substantielles sont obtenues pour des contraintes perpendiculaires à la fibre. Contrairement aux résultats basés sur des lois isotropes ou orthotropes dans la section transversale, le comportement polaire orthotrope réel mène à des gradients de contraintes prononcés sur toute la largeur de la section transversale.

Dans le rapport présent, le comportement mécanique d'une planche soumise à une tension perpendiculaire à la fibre et agissant sur les faces larges a été examiné. Un comportement cylindrique resp. polaire orthotrope, correspondant à un modèle de sciage réaliste de la planche, a été choisi comme loi de matériau. Un point d'effort central de cette recherche a été la détermination de l'effet de différentes conditions de chargement.

Il est démontré que le comportement mécanique d'une planche chargée transversalement dépend essentiellement des conditions aux limites qui restreignent resp. favorisent de manières différentes le couplage des contraintes normales et de cisaillement dans le cas de chargement „off-axis". Un modèle analytique simple idéalisant la section par un arrangement de ressorts parallèles et permettant la détermination du module d'élasticité apparent dans la direction perpendiculaire à la fibre est utilisé. Les résultats analytiques correspondent très bien aux résultats des éléments finis pour les conditions aux limites présentes à la mi-hauteur d'une section de bois lamellé.

KEYWORDS

Cylindrical material anisotropy of wood, solid wood board, glulam, tension perpendicular to grain, off-axis stress-strain relations, apparent transverse modulus of elasticity, influence of boundary conditions

1 INTRODUCTION

In general, the continuum modelling of wood resp. of glulam members and occasionally of solid lumber is based on plane stress assumptions and Cartesian or polar orthotropic constitutive laws, depending on the shape of the structure. One of the two principal material axes is the fiber direction coinciding i. g. with the beam axis. The other axis points normal to fiber resp. beam axis and is parallel to cross-sectional depth, i. e. quasi isotropic material behaviour within the cross-section is assumed. The elasticity coefficient $E_{\perp}$ in direction normal to the fiber axis is taken as a smeared mean of actually two distinct elasticity coefficients associated to radial and tangential growth directions; both values differ roughly by a factor of two. For the assessment of many aspects of the linear elastic structural behaviour of beams, the quoted 2dimensional approach is accurate enough. However, stresses perpendicular to the grain due to beam curvature or discontinuities such as holes and notches – actually strongly influenced by the cross-sectional polar anisotropy – are definitely not derived appropriately (Hanhijärvi and Ranta-Maunus, 1996; Ranta-Maunus, 1996). Deviating from solutions based on isotropic or orthotropic constitutive laws within the cross-section, the actual cylindrical resp. polar orthotropic behaviour results in pronounced stress gradients along the cross-sectional width. Related conclusions based on deepened investigations on this issue might lead to a reconsideration of the width effect as part of the volume effect.

In order to perceive the mechanical behaviour of glulam in tension perpendicular to the grain with respect to the influence of cylindrical anisotropy, a thorough understanding of the mechanics of a single board is mandatory. This paper deals with some aspects of cylindrical anisotropy and boundary conditions on stresses, strains and apparent off-axis stiffness of a wooden board subjected to tension perpendicular to the grain along the wide faces.

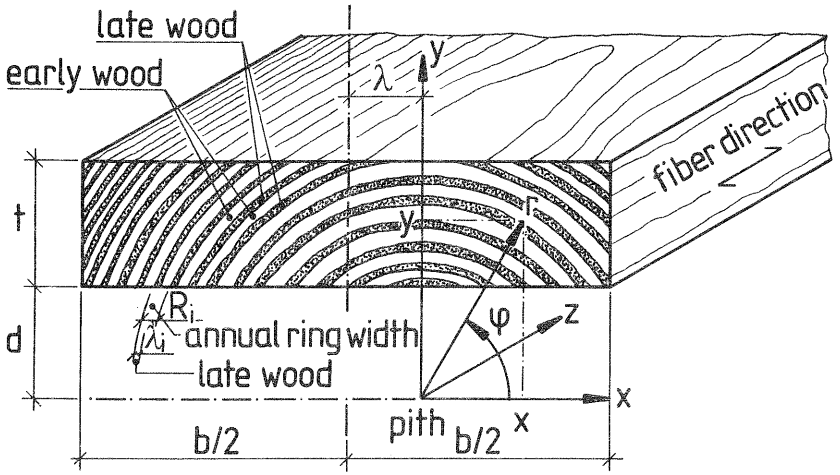

Fig. 1 Structural built-up of a wooden board from over-layered anisotropic conical resp. cylindrical early and late wood

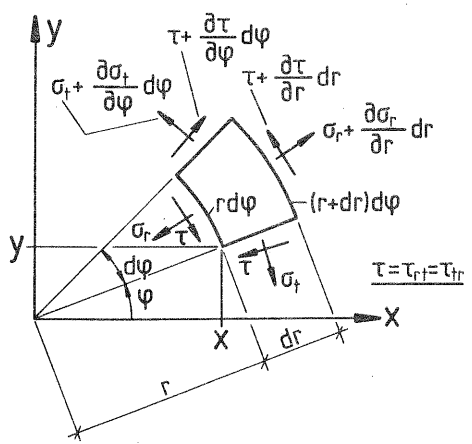

Fig. 2 Stress definitions in polar coordinates

The stresses can be derived in terms of a stress function F as (Girkmann, 1978)

$$\sigma_r = \frac{1}{r^2}\frac{\partial^2 F}{\partial \varphi^2} + \frac{1}{r}\frac{\partial F}{\partial r}, \qquad \sigma_t = \frac{\partial^2 F}{\partial \varphi^2}, \qquad \tau_{rt} = -\frac{\partial}{\partial r}\left(\frac{1}{r}\frac{\partial F}{\partial \varphi}\right) \qquad (3a\text{–}c)$$

where $\Delta\Delta F(r,\varphi) = 0$ and $\Delta = \frac{\partial^2}{\partial r^2} + \frac{1}{r^2}\frac{\partial^2}{\partial \varphi^2} + \frac{1}{r}\frac{\partial}{\partial r}$. (4a, b)

In this paper, stresses and strains are obtained primarily from numerical solutions for the governing differential equation (4) by finite element method.

2.3 Constitutive law

The polar orthotropic constitutive law is derived from the generalisation of Hooke's law $\varepsilon_{ij} = S_{ijk\lambda}\,\sigma_{ij}$ given by eq. (5) in its reduced form for rhombic material symmetry:

$$\begin{array}{lcccccccc}
\varepsilon_{11} & = S_{11}\,\sigma_{11} & + S_{12}\,\sigma_{12} & + S_{13}\,\sigma_{33} & 0 & 0 & 0 & \\
\varepsilon_{22} & = S_{21}\,\sigma_{11} & + S_{22}\,\sigma_{22} & + S_{23}\,\sigma_{33} & 0 & 0 & 0 & \\
\varepsilon_{33} & = S_{31}\,\sigma_{11} & + S_{32}\,\sigma_{22} & + S_{33}\,\sigma_{33} & 0 & 0 & 0 & \\
\varepsilon_{13} & = 0 & 0 & 0 & 0{,}5\,S_{44}\,\sigma_{13} & 0 & 0 & (5) \\
\varepsilon_{23} & = 0 & 0 & 0 & 0 & 0{,}5\,S_{55}\,\sigma_{23} & 0 & \\
\varepsilon_{12} & = 0 & 0 & 0 & 0 & 0 & 0{,}5\,S_{66}\,\sigma_{12} &
\end{array}$$

By setting r = 1, t = 2, z = 3 and introducing plane stress conditions ($\sigma_{i3} = 0$), using the reduced resp. technically familiar notations $\varepsilon_i = \varepsilon_{ii}$, $\sigma_i = \sigma_{ii}$ and $\sigma_{ij} = \tau_{ij}$, the polar orthotropic on-axis constitutive law becomes (for ε_z see below)

$$\begin{bmatrix} \varepsilon_r \\ \varepsilon_t \\ \varepsilon_{rt} \end{bmatrix} = \begin{bmatrix} S_{11} & S_{12} & 0 \\ S_{21} & S_{22} & 0 \\ 0 & 0 & S_{66}/2 \end{bmatrix} \begin{bmatrix} \sigma_r \\ \sigma_t \\ \tau_{rt} \end{bmatrix} \qquad (6)$$

or $\varepsilon = [S]\,\sigma$.

The on-axis compliances S_{ij} are related to the on-axis technical engineering constants by[2]

$$S_{11} = \frac{1}{E_r}, \quad S_{22} = \frac{1}{E_t}, \quad S_{66} = \frac{1}{G_{rt}}, \quad S_{12} = -\frac{\nu_{rt}}{E_t}, \quad S_{21} = -\frac{\nu_{tr}}{E_r}$$

and $$\frac{\nu_{rt}}{E_t} = \frac{\nu_{tr}}{E_r} .$$

Following, strain $\varepsilon_z = S_{31}\,\sigma_r + S_{32}\,\sigma_{22}$ with $S_{31} = -\nu_{zr}/E_r$ and $S_{32} = -\nu_{zt}/E_t$ is not considered further as usual in plane stress analysis with unrestrained deformation ε_z, which seems sufficient in this context.

2.4 Compliance resp. stiffness transformation into Cartesian off-axis coordinate system

The stress, strain, stiffness resp. compliance transformations in discrete points from the polar orthotropic on-axis material orientations to a rotated polar or Cartesian off-axis configuration is identical to transformation in pure Cartesian coordinates, as, in a point, polar coordinates may be replaced by Cartesian coordinates (Figs. 3a–c). The relations between Cartesian off-axis and polar on-axis stresses resulting from static equilibrium conditions are ($m = \cos\varphi$, $n = \sin\varphi$)

---

[2] Note that engineering for $S_{12} = S_{21}$ differ compared to some text book notations

$$\begin{bmatrix} \sigma_x \\ \sigma_y \\ \tau_{xy} \end{bmatrix} = \begin{bmatrix} m^2 + n^2 - 2mn \\ n^2 + m^2 + 2mn \\ mn - mn + \left(m^2 - n^2\right) \end{bmatrix} \begin{bmatrix} \sigma_r \\ \sigma_t \\ \tau_{rt} \end{bmatrix} \tag{7}$$

or $\quad \bar{\sigma} = [R]\,\sigma \quad .$

The on- vs. off-axis strain transformation in tensor notation is identical to stress transformation, i. e.

$$\bar{\varepsilon} = [\,R\,]\;\varepsilon \text{ where } \quad \bar{\varepsilon} = \left[\varepsilon_x, \varepsilon_y, \varepsilon_{xy}\right] \quad . \tag{8}$$

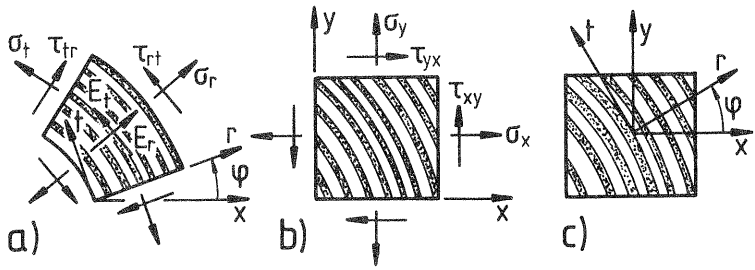

Figs. 3a–c Stress resp. coordinate transformation in a point from polar on-axis material coordinate system to Cartesian off-axis system
a) on-axis stresses **b)** off-axis stresses
c) definition of positive rotation

The constitutive relations in Cartesian off-axis coordinate system expressed by compliances then result from substituting ε in eq. (8) by eq. (6) and hence σ by inverted relation (7), giving

$$\bar{\varepsilon} = \left[\,\bar{S}\,\right]\,\bar{\sigma} \tag{9a}$$

where

$$\left[\overline{S}\right]=\left[\boldsymbol{R}\right]\left[\boldsymbol{S}\right]\left[\boldsymbol{R}\right]^{-1}=\begin{bmatrix} S'_{11} & S'_{12} & S'_{16} \\ S'_{21} & S'_{22} & S'_{26} \\ \frac{1}{2}S'_{16} & \frac{1}{2}S'_{26} & \frac{1}{2}S'_{66} \end{bmatrix} . \qquad (9b)$$

Alternatively, in terms of stiffness, the constitutive off-axis relations are:

$$\bar{\sigma}=\left[\overline{Q}\right]\bar{\varepsilon} \qquad \text{where} \qquad \left[\overline{Q}\right]=\left[\overline{S}\right]^{-1}=\left[\boldsymbol{R}\right]\left[\boldsymbol{S}\right]^{-1}\left[\boldsymbol{R}\right]^{-1} . \quad (10a, b)$$

In explicit notation, off-axis compliance coefficients S'_{ij} for the case of uniaxial loading by stress σ_y are:

$$S'_{12}=\cos^2\varphi\ \sin^2\varphi\left(\frac{1}{E_r}+\frac{1}{E_t}-\frac{1}{G_{rt}}\right)-\left(\cos^4\varphi+\sin^4\varphi\right)\frac{\nu_{rt}}{E_t} ,$$

$$S'_{22}=\frac{1}{E_y}=\cos^4\varphi\ \frac{1}{E_t}+\sin^4\varphi\ \frac{1}{E_t}+\cos^2\varphi\ \sin^2\varphi\left(\frac{1}{G_{rt}}-2\ \frac{\nu_{rt}}{E_t}\right) , \quad (11a\text{–}c)$$

$$S'_{26}=\cos\varphi\ \sin^3\varphi\left(\frac{2}{E_r}+2\frac{\nu_{rt}}{E_t}-\frac{1}{G_{rt}}\right)-\sin\varphi\ \cos^3\varphi\left(\frac{2}{E_t}+2\frac{\nu_{rt}}{E_t}-\frac{1}{G_{rt}}\right) .$$

Note that unsymmetrical matrix (9b) is based on tensor notation of strains delivering simpler transformation equations compared to the definition of (shear) strains in engineering notation, as stresses and strains transform equally and hence compliances and stiffnesses do too. This has to be borne in mind when comparing for instance the tensor quantities of the third row in eq. (9b) to those given in relevant textbooks (i. a. Tsai and Hahn, 1990).

The well known, most important feature of eqs. (9) and (10), is the so-called shear and normal strain i.e. stress coupling effect, meaning that normal and shear compliances are no longer uncoupled as in on-axis loading. So, for instance, unilateral off-axis loading in y-direction, apart from strains ε_x, ε_y, also evokes shear deformation ε_{xy}. Further, apparent off-axis MOE's E_x , E_y are strongly dependant on shear stiffness of polar on-axis configuration, which is illustrated exemplary by eq. (11b).

The latter effects are of eminent importance for the mechanical behaviour of a board resp. of glulam (staggered built-up of boards), when stressed in tension perpendicular to the grain on the wide side, which is shown in detail following.

3 RESULTS FOR APPARENT TRANSVERSE MOE RESP. STRESSES AND STRAINS DEPENDING ON BOUNDARY CONDITIONS

As an example, a board with a thickness of 33 mm, a width of 140 mm, symmetric built-up towards mid-width, i. e. with zero pith eccentricity ($\lambda = 0$) and a vertical pith distance of d = 33 mm is regarded (see Fig. 1). As polar orthotropic on-axis elasticity coefficients, the following values were chosen:

$E_r = 1000\ N/mm^2$, $E_t = 500\ N/mm^2$, $G_{rt} = 60\ N/mm^2$, $\nu_{rt} = 0{,}31$.

These values are well in line with those given for softwoods in literature (Koponen et al., 1991), however the upper limit applies implicitly to own results with glulam built up from boards with densities of $\geq 470\ kg/m^3$.

3.1 Analytical calculations with indeterminate boundary conditions

The apparent elasticity value E_y in a deliberate point x = r cos φ, y = r sin φ of a board in case of applied unit stress $\sigma_y = 1$ is

$$E_y(x,y) = 1 / \varepsilon_y(x,y) \qquad \text{where} \qquad \varepsilon_y(x,y) = S'_{22}(x,y) \qquad (12a, b)$$

and hence the course of E_y along width at constant depth y = const. = c. is denoted by

$$E_y(x,c.) = 1 / \varepsilon_y(x,c.) \quad . \qquad (12c)$$

The integral value of E_y in a line y = const. based on averaged strains along width b is

$$\overline{E_y}(c.) = 1 / \overline{\varepsilon_y}(c.) \qquad \text{where} \qquad \overline{\varepsilon_y}(c.) = \frac{1}{b} \int_b \varepsilon_y(x,c.)\, dx \quad . \qquad (13a, b)$$

Based on averaged strains over the thickness of the board, the variation of total apparent MOE $\overline{E_y}$ along width is defined by

$$\overline{E_y}(x) = 1 / \overline{\varepsilon_y}(x) \qquad \text{where} \qquad \overline{\varepsilon_y}(x) = \frac{1}{t} \int_t \varepsilon_y(x,y)\, dy \qquad (14a, b)$$

and hence total or integral apparent MOE $\overline{E_y}$ follows from

$$\overline{E_y} = 1 / \overline{\varepsilon_y} \qquad (15a)$$

where

$$\overline{\varepsilon_y} = \frac{1}{b\,t} \int_b \int_t \varepsilon_y (x, y)\, dy\, dx = \frac{1}{b} \int_b \overline{\varepsilon_y}(x)\, dx \quad . \tag{15b}$$

Note that completely different results are obtained for integral MOE's in a line or for the whole board, when the derivation is not based on the integrals of the compliances but on the integrals of the local stiffnesses along lines or areas, i. e.

$$\overline{S_y}(c.) = \frac{1}{b} \int_b E_y(x, c.)\, dx \neq \overline{E_y}(c.) \tag{16a}$$

and

$$\overline{S_y} = \frac{1}{b\,t} \int_b \int_t E(x, y)\, dy\, dx \neq \overline{E_y} \quad . \tag{16b}$$

Fig. 4 shows the course of $\overline{E_y}(x)$ acc. to eq. (14a) as a solid line. Rather identical results are obtained for MOE's at mid-depth y = c. = d + t/2 acc. to eq. (13a)[3]. The given curve mirrors the extreme influence of the shear modulus in off-axis loading: $\overline{E_y}(x)$ decreases rapidly from $E_y = E_r$ to values well below the tangential MOE E_t ; a recovery of the right hand tail of the $E_y(x)$ curve in Fig. 4 to the approximate value of the tangential MOE would be obtained in this configuration for a board width of about 240 mm.

The integral values acc. to eqs. (13a) and (15a) with c. = t/2 resemble very closely and deliver $\overline{E_y} = \overline{E_y}(t/2) \approx 290\ N/mm^2$. This value is

[3] Following $y = c. = d + t/2$ is abbreviated as $c. = t/2$, i. e. the off-set term „ $+ d$" is left aside.

obvi ously not the integral below the given curves for $\overline{E_y}(x)$. The integration over local MOE's acc. to eqs. (16a, b) would instead deliver the higher stiffness quantities of $\overline{S_y}(c.) \approx \overline{S_y} \approx 365\ N/mm^2$. The other curves given in Fig. 4 apart from the analytical solution refer to FEM computed results discussed in detail in the following chapter.

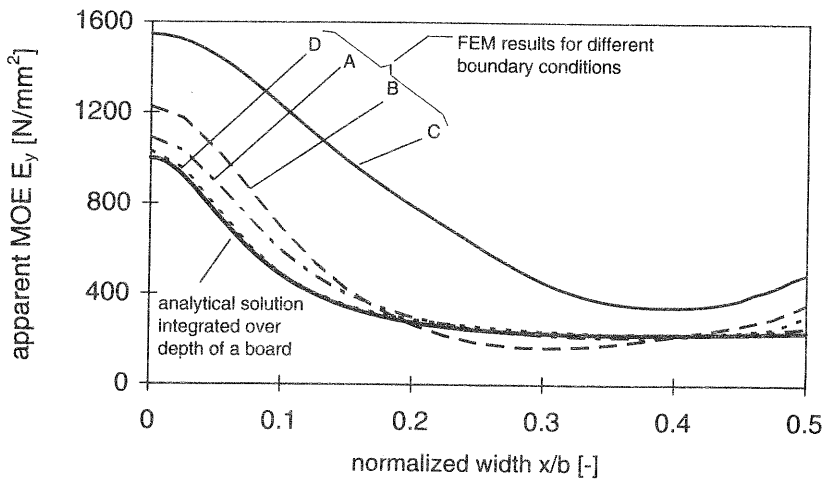

Fig. 4 Apparent MOE E_y (x) due to analytical calculation and according to FEM calculations for different boundary conditions A–D (see Fig. 6)

3.2 Finite element determination

For the finite element simulation of the off-axis stiffness, several approaches may be taken.

Closely related to the analytical determination of E_y(x,c.) resp. $\overline{E_y}(c.)$ via eqs. (12c) and (13a), for instance at edge y = c. =t/2, this edge

can be modelled as shown in Fig. 5 by a very thin layer of multiple adjacent finite elements showing the respective polar elasticity coefficients as the simulated line. In this investigation, the board width was divided into 80 elements; element thicknesses in the range of 1/300 to 1/30 of board thickness (here 0,1–1 mm) showed no marked influence on the results. The obtained $E_y(x,t/2)$ distribution is insensitive to application of load either as uniform line load or as imposed even displacement and coincides with the analytical solution for $E_y(x,t/2) \approx \overline{E_y}(x)$ as given in Fig. 4.

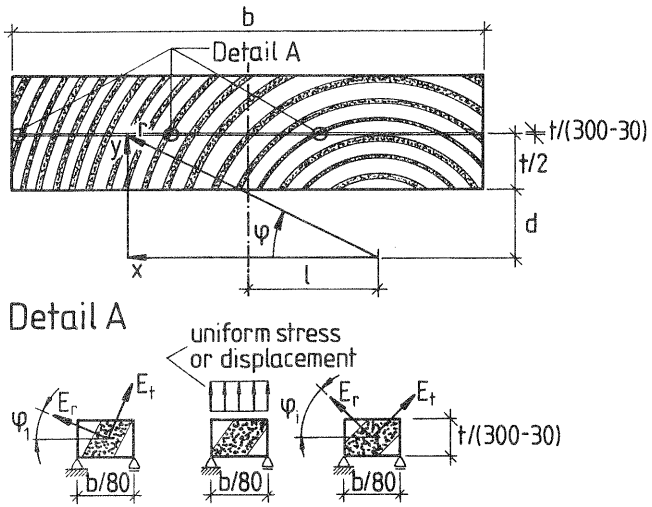

Fig. 5 Finite element determination of stiffness distribution along width at deliberate board depth (here: y = c. = t)

The determination of the apparent MOE's of the board, either along a line at constant depth ($E_y(x, c)$ resp. $\overline{E_y}(c)$), or as integral value over board thickness ($\overline{E_y}(x)$ resp. $\overline{E_y}$), and based on consideration of the actual contin-

uum, is strongly influenced by loading resp. support boundary conditions. Four configurations A–D, depicted by Figs. 6a–d were studied:

- configurations A and B: uniform line resp. displacement load at one edge, uniform vertical line support at opposite edge (Figs. 6a, b)
- configuration C: the board is glued between two stiff steel plates, loaded resp. supported centrally or uniformly(Fig. 6c)
- configuration D: the loading conditions depict the situation of a board located at mid-depth of a glulam cross-section built up from 16 boards with equal sawing patterns and on-axis stiffnesses acc. to specifications given in chap. 3; the edges along the width of the glulam prism are loaded resp. supported uniformly (Fig. 6d).

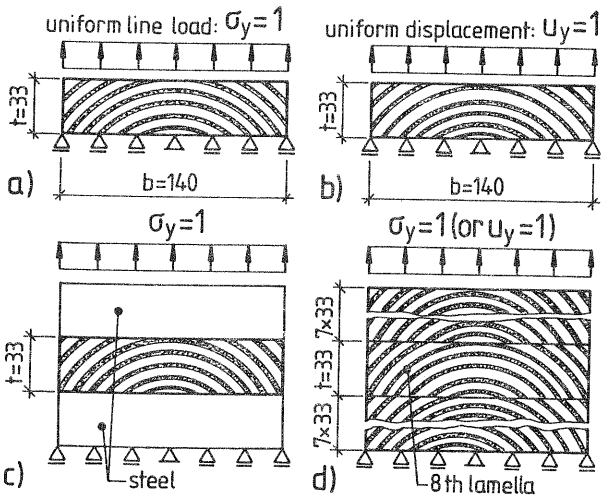

Fig. 6 Investigated loading boundary conditions in FEM based determination of transverse stiffness resp. stresses and strains:

a), b) uniform stress resp. displacement at edge c. = t

c) load transfer via stiff steel plates

d) loading conditions at mid-depth of a glulam cross-section (here 8th lamella)

The determination of the E_y distribution along width either on a line y = c. or based on averaged strains over board thickness now, contrarily to eqs. (13a), (14a), now has to incorporate the variation of stress, here in general no longer a unit quantity, i.e. Hooke's law gives:

$$E_y\,(x, c.) = \sigma\ (x, c.) / \varepsilon_y\,(x, c.) \tag{17a}$$

and

$$\overline{E_y}(x) = \sigma(x,t) \;/\; \overline{\varepsilon_y}\,(x) \tag{17b}$$

where $\overline{\varepsilon_y}\,(x)$, based on FEM derived strains $\varepsilon_y\,(x, y)$, is determined from eq. (14b).

Further, the integral MOE $\overline{E_y}$ is, in all cases of applied unit loading and for the analytical solution by eqs. (15a, b), given as integration over stress variation in width direction x and delivers a unit quantity. In case of imposed unit displacement, the integral MOE is derived from

$$\overline{E_y} = \frac{1}{b\,\overline{\varepsilon_y}} \int_b \sigma_y\,(x,t)\,dx = \frac{1}{b} \int_b \overline{E_y}\,(x)\,dx \tag{18}$$

with $\overline{\varepsilon_y}$ acc. to eq. (15b) based on FEM derived strains $\varepsilon_y\,(x, y)$.

Figs. 7a, b to 10a, b depict the results of the four investigated configurations A–D. In detail, Figs. 7a to 10a give the stress and strain distributions at mid-depth $\sigma_y\,(x, t/2)$, $\varepsilon\,(x, t/2)$, the stress along the top edge $\sigma_y\,(x, t)$ and the distribution of the integrated strain $\overline{\varepsilon_y}\,(x)$ acc. to eq. (14b). Figures

7b to 10b depict the related distributions resp. quantities of apparent MOE's $E_y(x, t/2)$, $\overline{E_y}(x)$, $\overline{E_y}$ acc. to eqs. (17) and (15) or (18).

In case of configuration A with uniform loading along edge c. = t, the stress $\sigma_y(x, c.)$ across board width remains nearly uniform, as shown for mid-depth c. = t/2 (Fig. 7a). Thus, the varying stiffness within the board is fully revealed by the variation of the local resp. integrated strains $\varepsilon_y(x, t/2)$, $\overline{\varepsilon_y}(x)$, both resembling each other closely. The obtained distributions for the apparent MOE's (Fig 7b) either at mid-depth or integrated over board thickness, $E_y(x, t/2)$ resp. $\overline{E_y}(x)$, consequently correspond closely and apart from mid-width fit quite well to the analytical solution (compare Fig. 4). In the case of configuration A, the mean value of the apparent MOE $\overline{E_y}$ = 297 N/mm² for the whole board cross-section is only marginally different from the aforegiven analytical solution: $\overline{E_y}$ = 290 N/mm².

In case of configuration B with uniform displacement loading along edge c. = t, strain distributions at different board depths are rather constant, however more differentiated than the analogous σ_y variations in constant load configuration A. Now, pronounced variations of stress along width are obtained with qualitatively similar shapes of the curves at different depths, for instance at c. = t/2 and c. = t. The curves given for $\sigma_y(x, t/2)$ and $\sigma_y(x, t)$ show pronounced stress peaks at mid-width and flat tails with minimal stress values near both edges ± b/2.

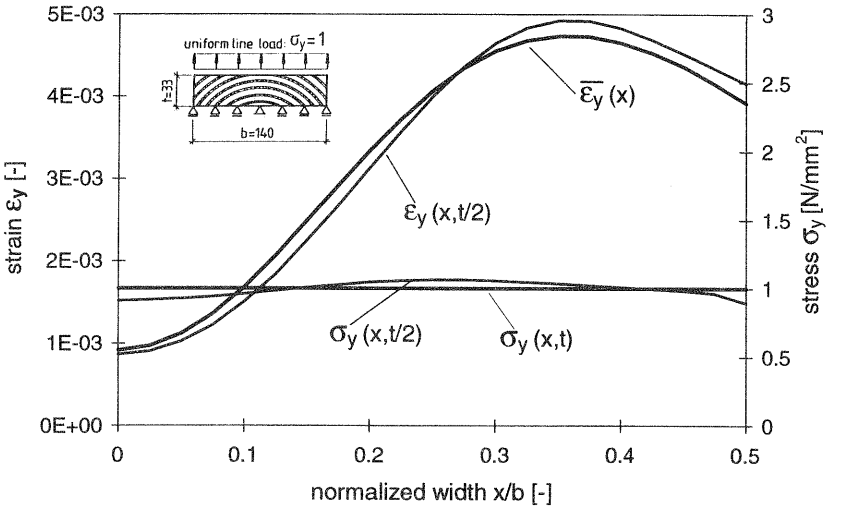

a)

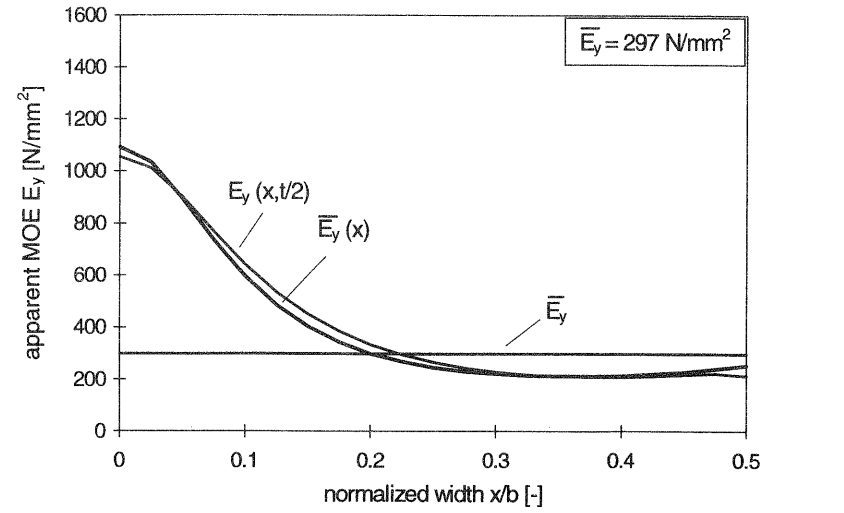

b)

Fig. 7 a, b Stress, strain and MOE distributions of a board loaded perpendicular to the grain by uniform line loading
a) $\sigma_y(x,t)$, $\sigma_y(x,t/2)$, $\bar{\varepsilon}_y(x)$, $\varepsilon_y(x,t/2)$ **b)** $\bar{E}_y(x)$, $E_y(t/2)$, $\bar{E}_y$

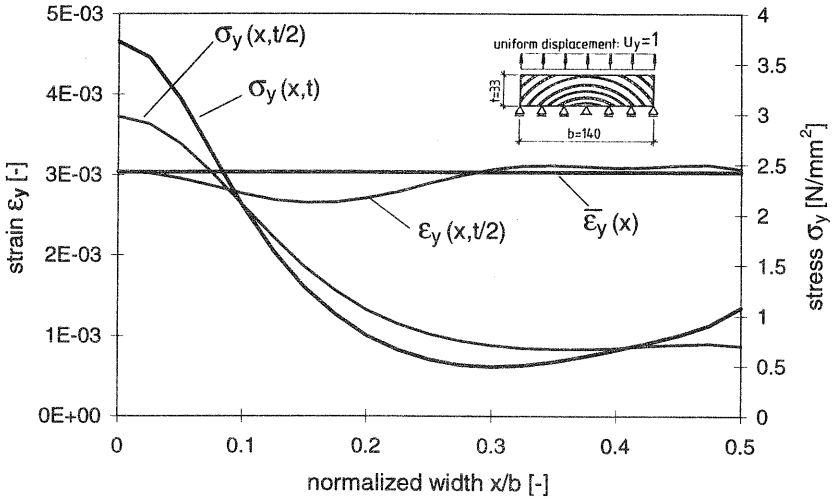

a)

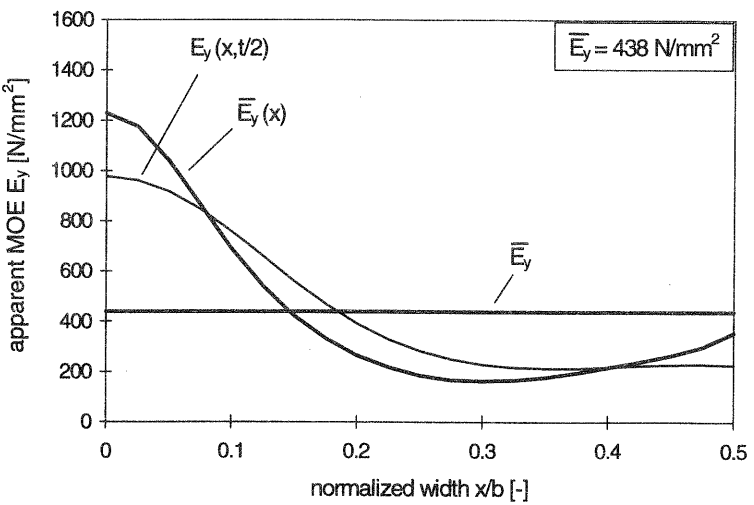

b)

Fig. 8 a, b Stress, strain and MOE distributions of a board loaded perpendicular to the grain by uniform displacement loading
a) $\sigma_y(x,t)$, $\sigma_y(x,t/2)$, $\bar{\varepsilon}_y(x)$, $\varepsilon_y(x,t/2)$ **b)** $\bar{E}_y(x)$, $E_y(t/2)$, $\bar{\bar{E}}_y$

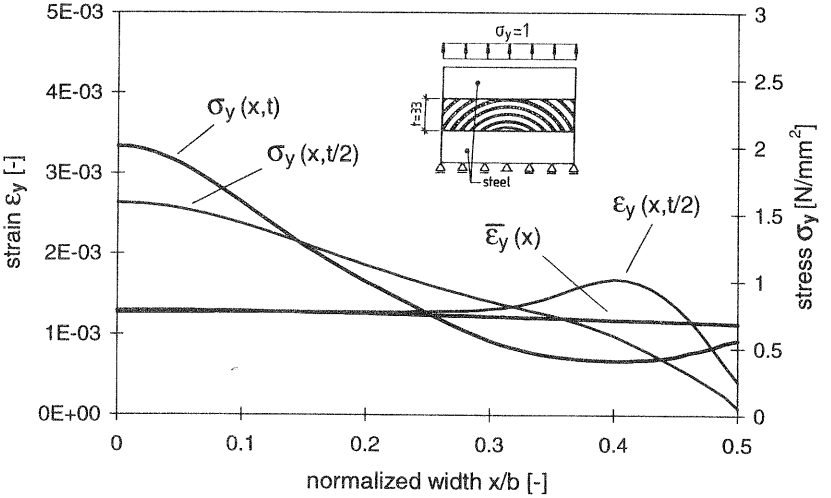

a)

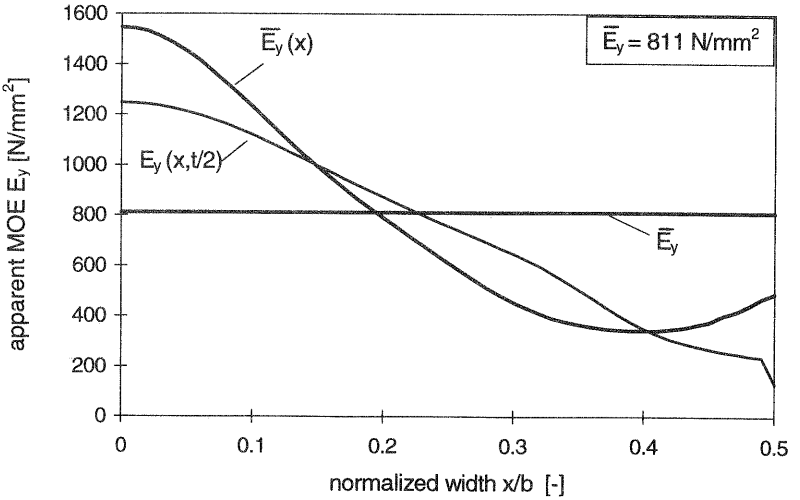

b)

Fig. 9 a, b Stress, strain and MOE distributions of a board loaded perpendicular to the grain through adhered steel plates
a) $\sigma_y(x,t)$, $\sigma_y(x,t/2)$, $\bar{\varepsilon}_y(x)$, $\varepsilon_y(x,t/2)$ **b)** $\bar{E}_y(x)$, $E_y(t/2)$, $\bar{E}_y$

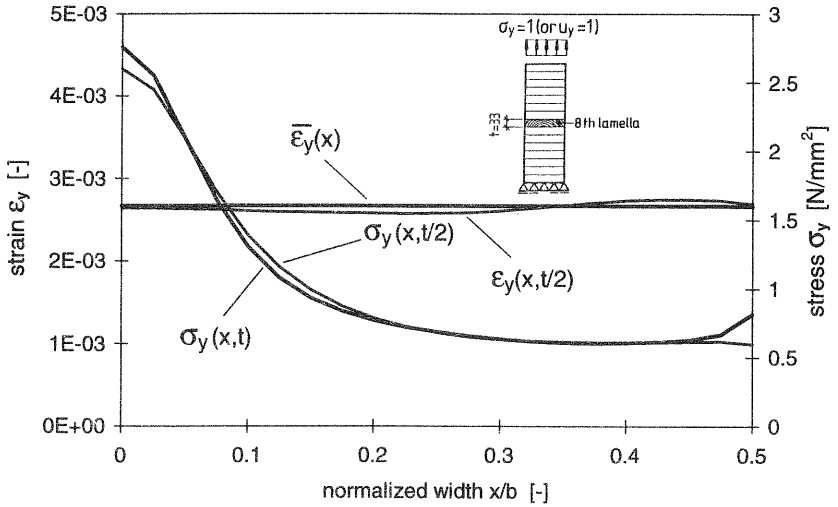

a)

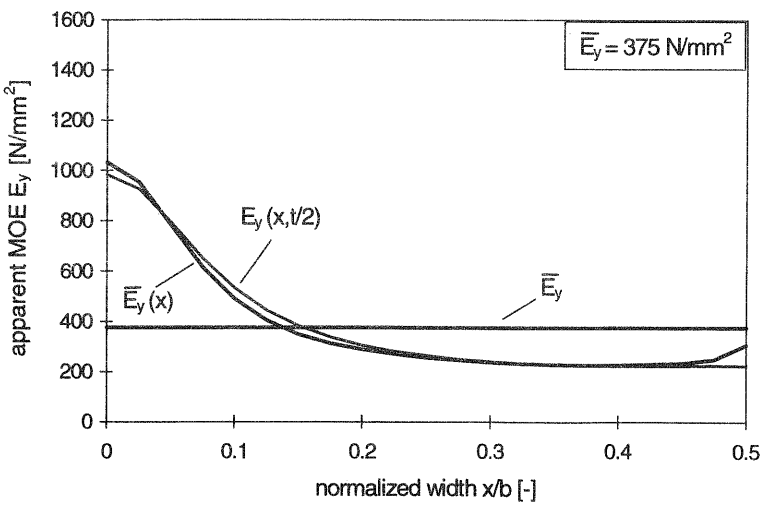

b)

Fig. 10 a, b Stress, strain and MOE distributions of a board within a glulam cross section loaded perpendicular to the grain
a) $\sigma_y(x,t)$, $\sigma_y(x,t/2)$, $\bar{\varepsilon}_y(x)$, $\varepsilon_y(x,t/2)$ **b)** $\bar{E}_y(x)$, $E_y(t/2)$, $\bar{E}_y$

The related courses of apparent MOE's $E_y(x, t/2)$ and $\overline{E_y}(x)$ are given in Fig. 8b. The MOE distributions are qualitatively similar to the analytical solution but show significant quantitative differences (see Fig. 4 for comparison of $\overline{E_y}(x)$ curves); the integrated overall value $\overline{E_y} = 438$ N/mm^2 obtained for configuration B is about 45 % higher compared to the analytical value.

Loading configuration C with load application via stiff steel plates delivers in a very rough approximation qualitatively similar ε_y, σ_y and E_y distributions as obtained for imposed uniform displacement (configuration B), however magnitudes of all quantities differ strongly. As for configuration B, the integrated strain $\overline{\varepsilon_y}(x)$ is constant along board width (Fig. 9a); however, the local strain distribution, for instance at mid-depth, $\varepsilon_y(x, t/2)$, shows a more pronounced deviation from the integral curve, especially towards the edges $\pm$ b/2, than in case of configuration B. The stress distributions at different depths, $\sigma_y(x, t/2)$, $\sigma_y(x, t)$, are similar in the middle part of the board's width (Fig. 9a), but towards the edges $\pm$ b/2, the stress gradients differ increasingly. The related MOE distributions given in Fig. 9b reflect the shape of the stress curves. The integrated overall MOE value $\overline{E_y} = 811$ N/mm^2 now is 1,85 times higher compared to configuration B. The extremely high $\overline{E_y}$ value results from the specific boundary conditions preventing nearly all shear deformations and further restricting horizontal transverse deformations in the vicinity of the plates. So, the apparent integral MOE value $\overline{E_y}$ in case of adhered steel plates, being rather unaffected by the normal and shear coupling effect, resembles roughly the average of the radial and tangential on-axis MOE's $(E_r + E_t)/2 = 750$ N/mm^2.

Loading configuration D, where the load is transferred to the board via other boards of equal elastic properties adhered to both sides (outermost boards loaded resp. supported uniformly), delivers nearly constant strain dis-

tributions along width at different depths of the board resp. for the whole board thickness (Fig. 10a). This nearly uniform state of strain ε_y results as hardly any restrictions of transverse and shear deformations are imposed to boards with sufficient distance to load application. Consequently, the stress distributions reflecting the variations of elasticity are similar to those of uniform deformation loading (case B), where rather uniform strain distributions were encountered, too; however on the contrary to case B, the stress curves along width at different depths c. = t/2 resp. t now almost completely coincide.

According to constant strain state and nearly equal stress variation at different depths, the apparent MOE curves $E_y(x, t/2)$, $\overline{E_y}(x)$ resemble closely and they correspond to the analytical solutions for $\overline{E_y}(x)$ (see Fig. 4). The latter involves that the vertical off-axis strain state in the board is only marginally influenced by stresses σ_x and τ_{xy}, i. e. $\varepsilon_y \approx S'_{22}\,\sigma_y$. This means that the board in configuration D can be perceived as an independent arrangement of springs along width with roughly constant compliance resp. stiffness over the depth and hence $\overline{E_y} = \overline{S_y}$. The integrated overall MOE value $\overline{E_y}$ = 375 N/mm² differs only marginally from the analytical mean value $\overline{S_y}$ = 365 N/mm² derived from stiffnesses.

4 CONCLUSIONS

It is demonstrated in detail that the cylindrical anisotropy of wood has a strong influence on the mechanical behaviour of a board in case of tension perpendicular to the grain imposed to the wide faces of a board. The apparent transverse MOE $E_{t,90}$ and the stresses in transverse direction show a pronounced dependency on loading boundary conditions, differently restricting resp. enabling the coupling of normal and shear stress in the imposed off-axis loading mode.

A simple analytic model for determination of apparent transverse MOE perceives the board cross-section as composed of springs arranged in parallel, implying a rather constant state of strain throughout depth. In case of a board with a built-up resp. sawing pattern symmetric to the mid-width, the analytical results corresponds well with FEM results for boundary conditions acting a mid-height of a glulam cross-section. For boards with pith eccentricities, the stated simple model, due to increasing shear coupling effect, shall deliver less correspondence with FEM results, which will be investigated further.

The derived stress variations, with a pronounced non singular stress peak within the cross-section, confirm recent Finnish investigations focused on the same problem. Not regarding the fact that further research has to be accomplished, it shall be stated that computations of tension stresses perpendicular to the grain which are not based on cylindrical anisotropy, certainly underestimate the failure relevant stress level in structures.

5 REFERENCES

Aicher, S., Dill-Langer, G. (1995): Tension strength perpendicular to the grain of supreme quality glulam conforming to CEN strength classes GL 32 and GL 36. Otto-Graf-Journal, Vol. 6, pp. 246–274

Dill-Langer, G., Aicher, S., Reinhardt, H. W. (1996): Creep of glulam in tension perpendicular to the grain at 20 °C/65 % RH and at sheltered outdoor climate conditions. Proceed. Int. Conf. on Wood Mechanics, pp. 155–173, Stuttgart

Girkmann, K. (1978): Flächentragwerke. Springer-Verlag Wien, New York

Hanhijärvi, A., Ranta-Maunus, A. (1996): Computational analysis of the effect of transverse anisotropy and annual ring pattern in cross-sections of curved glulam beams in the size effect of strength. Proceed. European Workshop on Application of Statistics and Probabilities in Wood Mechanics (in press), Bordeaux

Koponen, S., Toratti, T., Kanerva, P. (1991): Modelling elastic and shrinkage properties of wood based on cell structure. Wood Science and Technology, 25, pp. 25–32

Ranta-Maunus, A. (1996): The influence of changing state of stress caused by mechano-sorptive creep on the duration of load effect. Proceed. Int. Conf. on Wood Mechanics, pp. 187–201, Stuttgart

Tsai, S. W., Hahn, H. T. (1980): Introduction to Composite Materials. Technomic Publishing Company Inc., Lancaster